A NEW VIEW OF MARTIAN SURFACE GEOCHEMISTRY. V. E. Hamilton[1] and A. D. Rogers[2], [1]Southwest Research Institute, 1050 Walnut St., Suite 300, Boulder, CO 80302, hamilton@boulder.swri.edu, [2]Stony Brook University, 255 Earth & Space Sciences Building, Stony Brook, NY 11794, adrogers@notes.cc.sunysb.edu.

Introduction: We present new global maps of Martian surface chemistry (wt % oxide) calculated from Thermal Emission Spectrometer (TES)-derived mineral abundances. In doing so, we are able to quantitatively compare the TES data with chemistries measured in situ and in Martian meteorites and consider the implications for primary igneous and weathering trends [e.g., 1].

We also compare the spatial variations in TES-derived chemistry with variations in global elemental maps measured from orbit by from the Gamma Ray Spectrometer (GRS) suite [2].

Methods: [3] derived global phase distributions from thermal infrared spectra acquired by TES. The focus of that study was global variations in olivine solid solution composition. Here, we use their complete global mineralogy results to calculate major element chemistries.

Phase abundance data. Phase abundances were obtained for individual (~3 x 6 km) TES pixels by linear least squares fitting of TES-measured Martian spectra with a spectral library of 41 geologic phases and atmospheric components [3]. Atmospheric component abundances are subtracted and the remaining surface phase abundances are normalized to 100%. These are assumed to represent fractional abundance (vol %) of the surface materials [e.g., 4].

Calculation and mapping of wt % oxides from TES phase abundances. Volumetric abundances of each identified phase in a pixel are converted to weight percent by dividing by the density associated with that phase and normalizing fractions to 100%. Wt % oxides for each phase [5] are multiplied by the modeled weight fraction of that phase and combined to produce the derived "whole rock" chemistry for each pixel. Values are calculated on a CO_2- and H_2O-free basis. Uncertainties for TES 10 cm^{-1} sampling data (in wt %) are: SiO_2 = 1.5, Na_2O = 0.4, K_2O = 0.4, CaO = 0.8, MgO = 2.4, FeO* = 1.2, and Al_2O_3 = 1.7 [6].

Results & Discussion: *Geographic variability.* Qualitatively, our new TES-derived major element maps (2 ppd) display geographic variations that correlate well with geographic variations in lithology observed by [7]. The lithologic maps of [7] are based upon statistically separable variations in TES spectral shapes, rather than on derived mineralogy as in this work. These two methods are independent, and the fact that spatial variations in our maps correspond with variations in their maps indicates that both analytical approaches yield similar answers, which should be expected, but is nonetheless satisfying to confirm. Quantitatively, some regions show differences in average wt % oxides. Syrtis Major has lower average K_2O (0.5 wt%) than Acidalia Planitia (1.1 wt %). Acidalia Planitia has lower average MgO (8.4 wt %) than Syrtis Major (10.8 wt %). Acidalia also exhibits higher Al_2O_3 (12.1 wt%) than Hesperia Planum (10.0 wt %) and Erythraeum Planitia (9.5 wt %).

Igneous classification. On the igneous classification diagram that plots abundances of wt % silica (SiO_2) vs. wt % alkalis (Na_2O+K_2O) [8], our global chemistries plot in an oval, bullseye-type, density cloud similar to that of [1]; our SiO_2 wt% range is similar, but the distribution exhibits a shallower positive slope, having a smaller, and lower, range of alkali values (**Figure 1**). The likely origin of this difference is alkali feldspar (microcline) and micas (biotite, muscovite) in the spectral library of [1]; inclusion of small amounts of these phases in the fits to the TES spectra would increase alkali values in their data relative to ours. A plot of FeO*/MgO vs. SiO_2 demonstrates anhydrous vs. hydrous igneous fractionation trends; our data exhibit slightly increased FeO*/MgO relative to the data of [1]. A possible origin of this difference is the use of the pyroxene pigeonite in our spectral library. Pigeonite is commonly identified in our TES analysis, but was not included in the spectral library used by [1] and is substantially more Fe-rich than the low-Ca pyroxenes (enstatite and bronzite) in their library. Olivine composition is a potential source of the differences in FeO*/MgO, but both studies used similar sets of Mg-Fe olivines, so it seems more likely that pigeonite explains the differences in this ratio.

Weathering trends. A ternary plot showing the relationship between Al_2O_3, FeO+MgO, and CaO+Na_2O+K_2O (in mol %) has been used to describe weathering trends on Mars [9]. Martian in situ measurements do not follow terrestrial weathering trends (which tend to decrease in CaO+Na_2O+K_2O and increase in Al_2O_3), but instead follow a generally linear trend whereby FeO+MgO decreases with increasing alteration/weathering. This trend has been interpreted as consistent with acidic alteration of basaltic rocks and the dissolution of olivine [9]. Our data plot in a cloud that overlaps the proposed Martian weathering trend demonstrated by in situ measurements (**Figure 2**) [9]. However, variations in FeO*+MgO occur in unweathered basaltic rocks, and other Martian weathering

trends are observed (e.g., removal of $CaO+Na_2O+K_2O$ in Wishstone- and Watchtower-class rocks) [9], so we also are looking at regional data.

General chemical trends. Plots of wt % oxide vs. SO_3 [e.g., 10] show that global values obtained from TES generally overlap soil values measured in situ by the Viking, Pathfinder, and MER landers/rovers. TiO_2 is generally lower (<0.5 wt%) than values measured in situ, where TES-derived abundances are likely to be underestimates of the true values. The primary titanium-bearing phase in the TES mineral library used in this study is an augite containing 1.03 wt % TiO_2 [11]. Ilmenite is a common repository of Ti in basaltic rocks, but was not included in the spectral library; however, typical abundances of this phase are likely too small to be reliably identified by TES from orbit. Assuming ilmenite is present but unidentified, TiO_2 will be underestimated. Iron from ilmenite also will go unidentified, but the contribution to FeO* from iron in ilmenite is small. TES-derived abundances of CaO are higher than values measured in situ, by up to a factor of two. Our wt % CaO includes contributions from sulfate but apparently is not as well correlated with SO_3 globally as it is in local soils (because Ca also is common in silicates that vary in abundance globally).

Comparison to GRS. Maps of TES- and GRS-derived major element abundances are broadly consistent in their ranges of observed wt % oxide values and show relative agreement at global scales (despite the significant differences in their penetration depths), but greater variations at regional scales. Silicon is elevated in the northern lowlands in both data sets; an equivalent mid-latitude enrichment in silica measured by GRS is weaker in the TES map. Iron is low in equatorial regions relative to the northern lowlands in both datasets, but GRS shows relatively more Fe in Syrtis Major as compared to the adjacent materials whereas TES shows a relative low as compared to adjacent materials. Potassium shows relatively low abundances at low latitudes compared to the northern lowlands; at regional scales, trends are similar in some places (low in Syrtis Major) and differ in others (eastern Cimmeria moderate in GRS, low in TES). H_2O varies most strongly with latitude in TES map, whereas GRS distribution shows stronger longitudinal variation.

Ongoing work: We currently are producing data sets that are normalized to exclude contributions from weathering phases. These new data will enable us to evaluate the contributions of weathering phases to global geochemistry. In addition, we are working on quantitative comparisons of TES-derived major element abundances to those derived from the GRS.

References: [1] McSween Jr., H. Y., et al. (2009) *Science, 324*, 736. [2] Boynton, W. V. et al. (2007) *JGR, 112*, doi:10.1029/2007JE002887. [3] Koeppen, W. C. and Hamilton, V. E. (2008) JGR, 113, doi: 10.1029/2007JE002984. [4] Hamilton, V. E. and Christensen, P. R. (2001) *JGR, 105*, 9717. [5] Christensen, P. R. et al. (2000) *JGR, 105*, 9735. [6] Hamilton, V. E. et al. (2001) *JGR, 106*, 14,733. [7] Rogers, A. D. and Christensen, P. R. (2007) *JGR, 112*, doi:10.1029/2006JE002727. [8] LeBas, M. J. et al. (1986) *J. Pet., 27*, 745. [9] Hurowitz, J. A. et al. (2006) *JGR, 111*, doi: 10.1029/2005JE002515. [10] Yen, A. S. et al. (2005) *Nature, 436*, 49. [11] Hamilton, V. E. (2003) *JGR, 108*, doi:10.1029/2003JE002052.

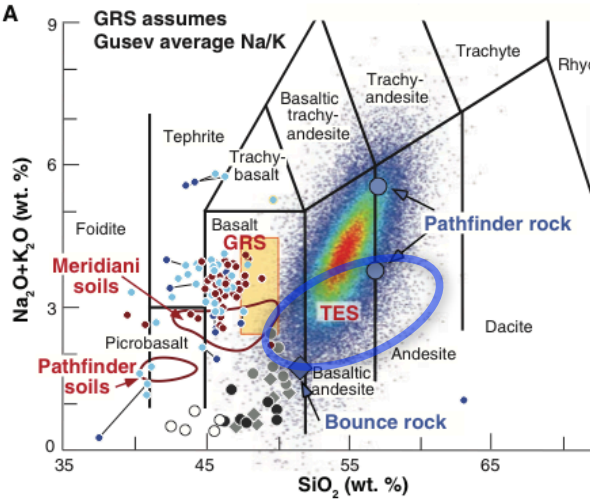

Figure 1. Silica vs. alkalis from this work (blue oval) overlaid on data from [1] (their Figure 2a).

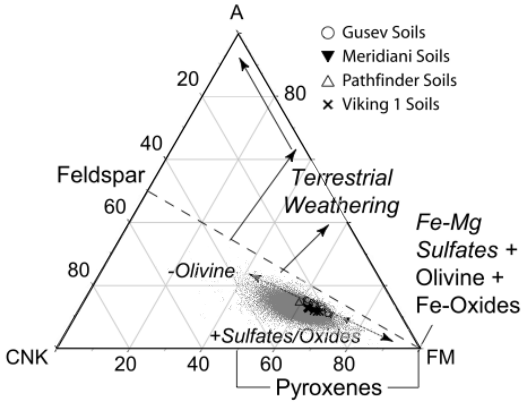

Figure 2. Ternary plot (in mol %) showing TES-derived chemistries for low-albedo (<0.20) regions (gray cloud) overlaid on in situ data (symbols) compiled by [9] (their Figure 14). TES data fall along the Martian acid weathering trend, but primary igneous and other weathering trends may be present in the global data.